Solar Energy Materials and Solar Cells 199 (2019) 83–90

Contents lists available at ScienceDirect

Solar Energy Materials and Solar Cells

journal homepage: www.elsevier.com/locate/solmat

Enhanced efficiency for building integrated concentrator photovoltaic modules based on rare earth doped optics

Joseph Day*, S. Senthilarasu, Tapas K. Mallick

Environment and Sustainability Institute, University of Exeter, Penryn Campus, Cornwall, TR10 9FE, UK

ARTICLE INFO

Keywords:
Building integrated PV
Concentrating PV
Efficiency
Nanomaterials
Rare earth ions
Spectral conversion

ABSTRACT

A major challenge facing silicon solar cells used in building-integrated concentrator photovoltaics (BICPV) is their reduced electrical response when exposed to light of short or long wavelengths. In an attempt to tackle this problem, single cell static CPV modules were fabricated with some of the devices containing rare earth doped compounds which were dispersed into the system in varying concentrations and geometries. Under a solar simulator at 1000 W/m^2, the power conversion efficiency (PCE) of devices improved up to 11.1% relative through the addition of these materials. At lower irradiances and compared to cells without concentrators, the relative efficiency gains were more pronounced and external quantum efficiency (EQE) measurements suggested spectral conversion was responsible for these enhancements. For a large scale BICPV system, a simple analysis showed cost per watt could fall by up to 8.1% and power output increased from 25.7 to 28.4 W/m^2 through this approach.

1. Introduction

The use of concentrating optics together with photovoltaic (PV) cells can increase the number of incident photons on a cell and hence reduce the required area of active PV material to achieve the same power output [1]. Various systems have been proposed to realize the focusing of light [2–5] but an exciting opportunity is presented by 3-dimensional static concentrators based on a square elliptical hyperboloid (SEH) design [6]. These optics are facilely produced and don't require solar tracking, so could be a cost-effective route to low concentration silicon-based PV devices. Concepts for such modules contain an array of concentrators to give the added benefit of semi-transparency and thus are ideal candidates for building integrated systems which could form part of a window façade (as in Fig. 2a–c). However, to make these designs more competitive compared to other building integrated PV (BIPV) approaches, the efficiency must be maximized in order to increase power per unit area and lower cost per watt. The design and optical efficiency (power of the light transmitted through the base of the concentrator divided by the power of the incident illumination) of the SEH concentrator has been analyzed [6], therefore we must seek ways to reduces energy losses in the solar cell themselves.

Silicon solar cells, like all single junction PV technologies, suffer from fundamental losses in power conversion efficiency (PCE) due to the mismatch between the solar spectrum and band gap energy (E_G) of the cell [7]. Incident photons with $E < E_G$ are not able to generate photocurrent whereas those with $E > E_G$ do so but give the electrons excess energy which is dissipated as heat (the losses can be visualized in Fig. 1). Multi-junction solar cells are one way to overcome this by using multiple cells of differing E_G stacked on one another to absorb separate regions of the solar spectrum more effectively [8]. However, these high-efficiency devices are expensive to produce so are combined with high-level concentrators to reduce cost per watt, but a clear economic solution has yet to be delivered [9]. Spectral conversion therefore is an alternative approach which changes the properties of the incident photons, rather than the cell itself, by three luminescent processes: upconversion [10] (UC), downconversion [11] (DC) and downshifting [12] (DS). UC involves combining the energies of two low energy photons into one which surpasses the E_G whereas DC splits the energy of one high energy photon into two of lower energy and DS reduces the energy of a single photon. From Fig. 1 it can be seen all of these have the theoretical potential to increase solar cell performance through harnessing a greater portion of the sun's energy [13]. In reality these processes take place at a molecular level in materials such as dyes [14–16], quantum dots [17–19] and rare earth doped compounds [20–22] which are usually incorporated in a layer above, below or inside the PV cell [23–25].

A further area of interest is the combination of spectral conversion and concentrating optics to obtain the benefits of each, the inspiration

* Corresponding author.
E-mail address: jd553@exeter.ac.uk (J. Day).

https://doi.org/10.1016/j.solmat.2019.04.013
Received 30 November 2018; Received in revised form 9 April 2019; Accepted 12 April 2019
Available online 29 April 2019

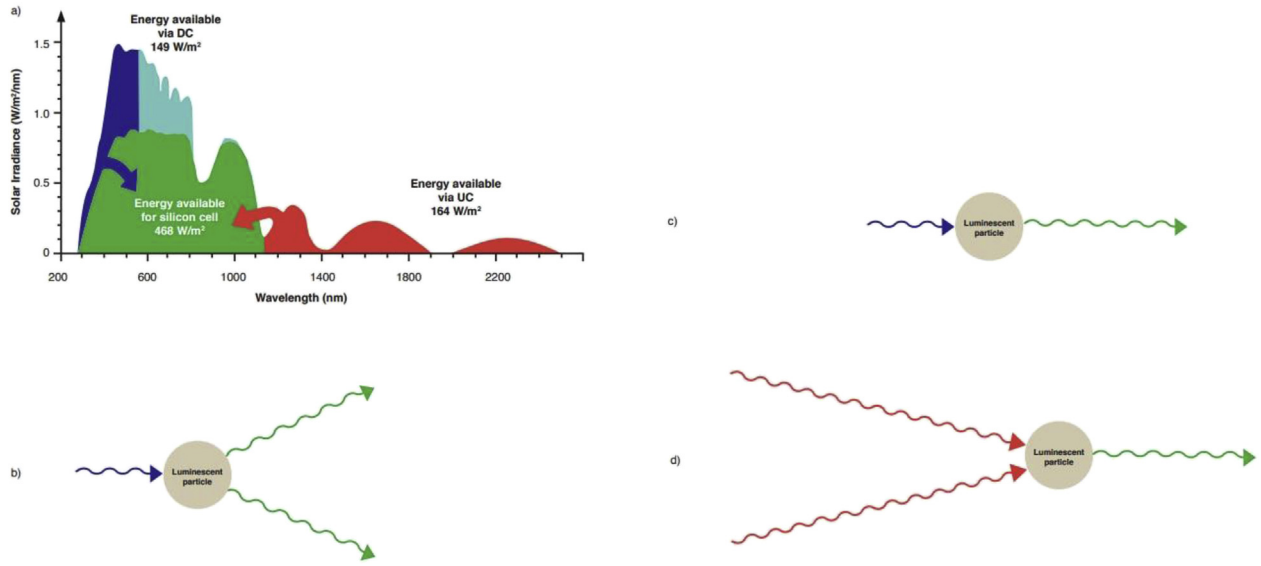

Fig. 1. Concept of spectral conversion for solar cells. a) Only the green shaded portion of the solar spectrum's energy (33%) is available for a silicon cell. However the blue and red portions can theoretically be harnessed via spectral conversion. b) A luminescent specie (LS) can absorb a single photon from the blue region and emit two photons in the green region. This is known as downconversion. c) An LS can also absorb a single photon from the blue region and emit a single photon in the green region. This is known as downshifting. d) Conversely an LS can absorb two photons from the red region and emit a single photon in the green region. This is called upconversion. (For interpretation of the references to colour in this figure legend, the reader is referred to the Web version of this article.)

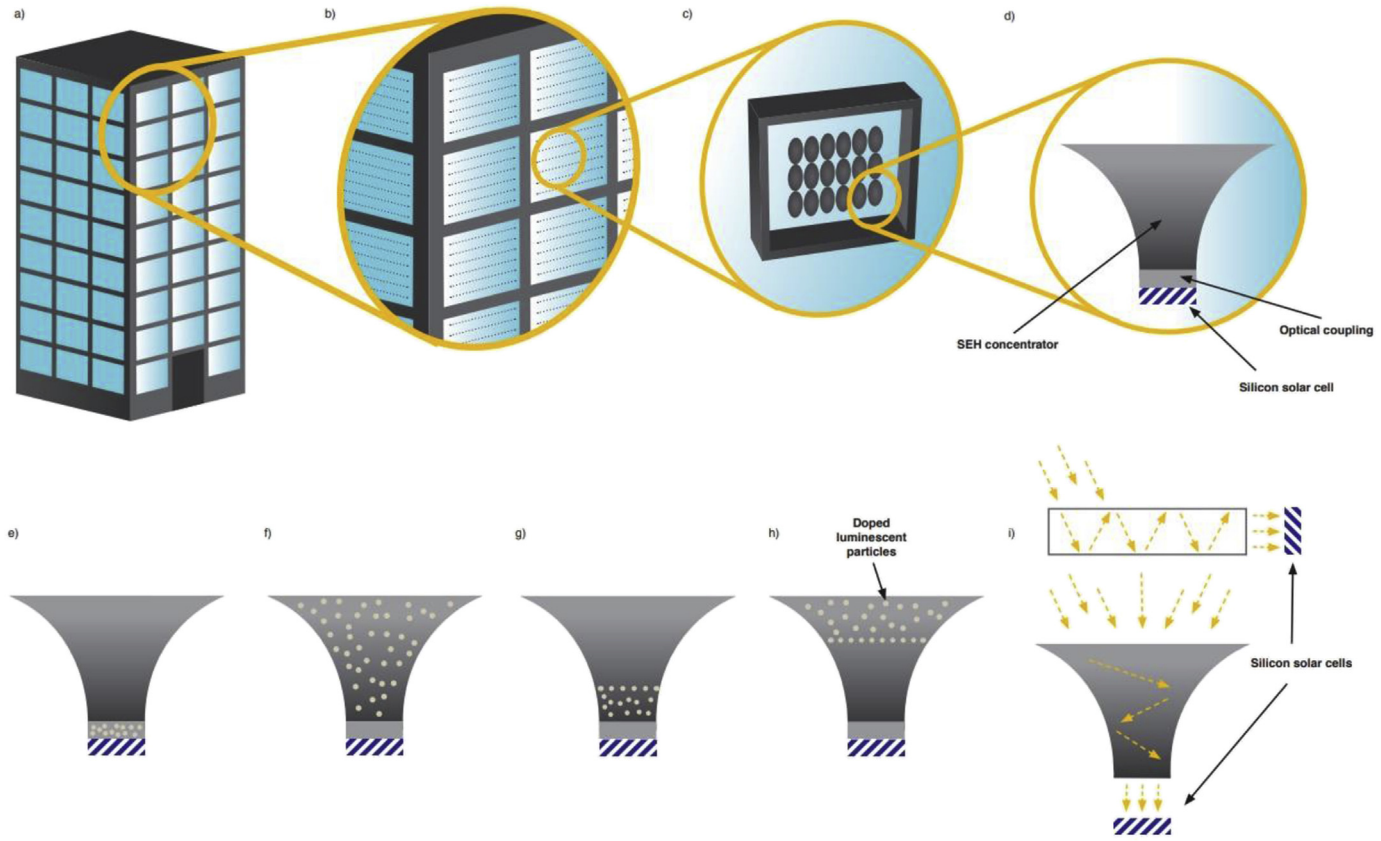

Fig. 2. Doped concentrators for building integrated photovoltaics. a) A south-facing building front in the northern hemisphere with several window facades b) A single window façade consisting of many CPV arrays. c) A single CPV array of 24 silicon cells and concentrators connected together to produce a power output. d) Cross-section of a single CPV module. e-h) doping of the rare earth compounds in the configurations used in this investigation: e) doped optical coupling f) homogenously doped concentrator g) bottom doped concentrator h) top doped concentrator. i) A luminescent solar concentrator which can also be building integrated into a window façade and works on a similar principle of total internal reflection. (For interpretation of the references to colour in this figure legend, the reader is referred to the Web version of this article.)

behind this study. One such device proposed in 1976 [26] which has been widely studied is the luminescent solar concentrator (LSC) with a pleasing aesthetic and potential for building integration [27]. LSCs tend to have a thin-cuboid shape and contain luminescent particles which absorb radiation and re-emit it towards PV cells at the edges by total internal reflection. However, despite recent progress [28–31] only modest efficiencies at larger scales have been attained, so it is important to explore alternative options. The SEH concentrators are also based on total internal reflection, so there is no reason why the same technique of introducing a luminescent materials could lead to enhanced performance of cell's coupled to these optics.

Therefore, four different methods of doping luminescent particles were proposed as can been in Fig. 2(e–h). The materials used were the rare earth doped compounds $NaYF_4$: Er^{3+}, Yb^{3+} and $Sr_4Al_{14}O_{25}$: Eu^{2+}, Dy^{3+} which were chosen because of their low cost and suitable absorption-emission profile for enhancing PV performance [32–34]. Single cell modules were fabricated based on the aforementioned designs containing either $NaYF_4$: Er^{3+}, Yb^{3+} or $Sr_4Al_{14}O_{25}$: Eu^{2+}, Dy^{3+} at fixed ratios of 0.1% w/w for the doped concentrators and varying levels of 0.25, 0.5, 1 and 2% w/w for the doped optical couplings. The devices were then characterized under a solar simulator to determine the power conversion efficiency and short circuit current density (J_{SC}), and compare these values to those for control devices (i.e. the same design but without any luminescent particles, Fig. 2d). Furthermore, characterization at lower irradiances (0.4, 0.6 and 0.8 suns) took place and a tunable laser was used to determine EQE profiles (the percentage of photons at a given wavelength that generates photocurrent), so it could be seen which parts of the solar spectrum were responsible for the PCE changes. Finally, PV cells without concentrators but the same doped couplings were studied, to investigate the effect of the optics. To the authors' knowledge, this is the first time a 3-dimensional static concentrator PV system of this shape has been doped with rare earth compounds for the aim of increased efficiency.

2. Materials and methods

2.1. Materials

The two rare earth doped compounds of 99.0% purity ($NaYF_4$: Er^{3+}, Yb^{3+} and $Sr_4Al_{14}O_{25}$: Eu^{2+}, Dy^{3+}) were purchased from Sigma-Aldrich. The quoted sizes of the particles were 1–5 μm for $NaYF_4$: Er^{3+}, Yb^{3+} and 180 mesh (74–88 μm) for $Sr_4Al_{14}O_{25}$: Eu^{2+}, Dy^{3+}. Preliminary studies showed the $Sr_4Al_{14}O_{25}$: Eu^{2+}, Dy^{3+} particles too large to be effectively incorporated, so they were ground via an agate mortar and pestle for 30 min. The 3-D concentrators were made from Crystal Clear® 200 casting resin and the optical coupling from Sylgard®184 silicone elastomer. Both of these have similar refractive indexes (1.50 and 1.42) and high transparency, so optical losses are minimized. Furthermore, when set, the casting resin is non-brittle and UV resistant, ideal properties for use in CPV. The solar cells used were provided by the National Renewable Energy Centre (NAREC) with an active PV area of 1 cm^2 and the following manufacturer stated electrical performance parameters under 1 sun (without a concentrator): PCE = 17%, J_{SC} = 36 mA/cm^2 and V_{OC} = 0.56 V.

2.2. Synthesis of concentrators and optical couplings

For the concentrators, parts A and part B of the casting were mixed at the ratio of 10:9. If a doped concentrator was required, the relevant rare earth doped compound was added to part B and dispersed by a magnetic stirrer prior to mixing with part A. A vacuum oven (MTI technologies EQ-DZF-6210 Vacuum Oven) was used to degas the mixtures at several stages to minimize the formation of air bubbles. Once mixed, the resin was poured gently into the casting mold which had been sprayed with Smooth-on Universal™ mold release (to aid with removal) before being degassed for a final time and left to cure at ambient temperature for 16 h. If a partially doped concentrator was needed, then the desired depths of the mold were filled with either doped or un-doped casting resin and a second layer added to fill the vessel. After curing, the concentrators were carefully removed from the mold by detaching the glass base and gently pushing them out through the top. The UV–Vis transmittance spectra of the concentrators under different doping configurations may be found in the supplementary material.

2.3. Synthesis of optical couplings

If an undoped optical coupling was required then the silicone elastomer was prepared by mixing part A and part B at the ratio of 10:1 as specified by the manufacturer. Similarly to the casting resin, degassing via vacuum oven was utilized to reduce bubble growth. For doped optical couplings, rare earth doped compounds were added to parts A and B at the given mass ratio, dispersed by a magnetic stirrer and then subjected to ultra-sonication (Hilsonic® ultra-sonicator) for 10 min (due to its high viscosity limiting the effectiveness of the stirring). The dopants were able to be added after A and B had been mixed together because of the longer pot life of Sylgard.

2.4. Fabrication of CPV and PV devices

To put the device together, cut squares of 3 mm thick Plexiglas® acrylic were used as a base and a glue gun (Loctite® Hot Melt) created a boundary so that the coupling would not leak from the sides. Solar cells with soldered contacts were placed on top of this base before being covered with a small quantity of silicone elastomer (doped or un-doped). Finally, the cured concentrators (doped or un-doped) were fixed above the solar cell, taking care to align the square base with the cell, and then left to set at room temperature for 48 h. If no concentrator was required, a similar quantity of the doped or un-doped optical coupling elastomer was drop cast on to the cells (see Fig. 3). For reliability, three copies of each specified design were fabricated. A flow diagram of the steps can be found in the supplementary information.

2.5. Material characterization

The claimed properties rare earth powder properties were to be verified by x-ray diffraction (Siemens D5000 Powder X-ray Diffractometer) and scanning electron microscopy (Hitachi S3200N SEM-EDS) analysis. The transmittance spectra of the doped Sylgard layers were obtained from UV/Vis/NIR spectrometry (PerkinElmer Lambda 1050). As expected a decrease in transmittance with increased doping level was observed. These figures may be found in the supplementary information.

2.6. Device electrical characterization

All the devices were characterized in air at a near constant temperature of 25 °C through the use of two illumination sources: a solar simulator (AAA Wacom® Super Solar Simulator) and tunable laser (Bentham PVE300). The solar simulator contains a xenon arc lamp which can replicate the AM 1.5G spectrum. The simulator is calibrated through Fraunhofer Institute, ISE, Freiburg, Germany through reference cell (WPVS, S/N 10510–0401). Both sources were calibrated with silicon reference cells to obtain appropriate currents of previously accepted values. Devices were placed on a horizontal platform beneath this and connected at both terminals via two metal clips to a current-voltage (I-V) tracer (EKO MP-160i) which can determine the electrical properties of the module including J_{SC}, $V_{OC,}$ PCE and an I-V curve. Two I-V tracer measurements were taken in 5-s sweeps, one after devices were illuminated for 30 s and one after 60 s to avoid any anomalies, while the high specification of the solar simulator ensured a stable I-V characteristic. The irradiance of the solar simulator could be modified

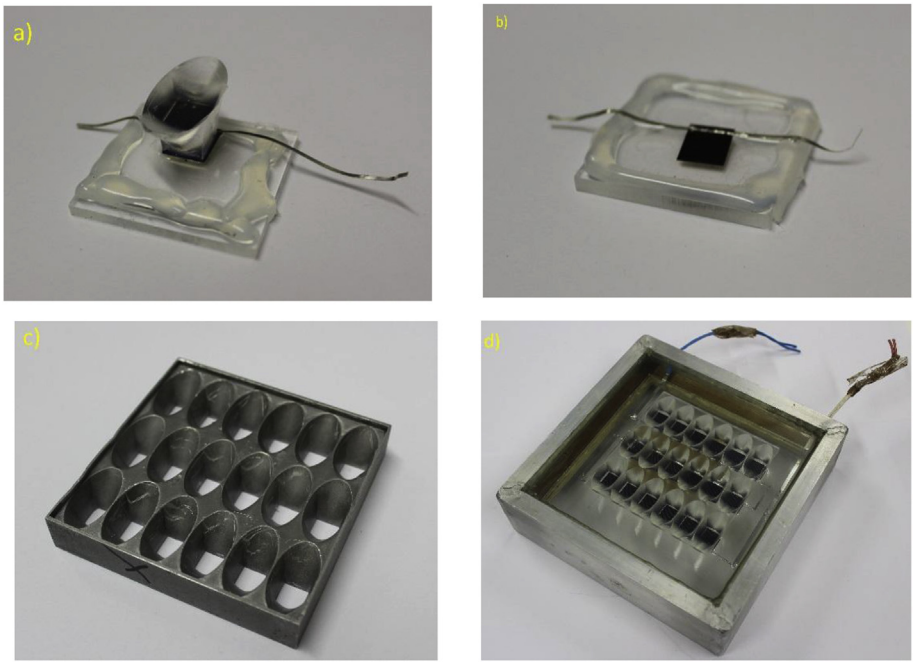

Fig. 3. Real life images of the devices surrounding this experiment. a) A completed single cell CPV module. b) A completed single cell PV module (without concentrator). c) The casting mold used to produce the concentrators. d) A prototype array of CPV cells which could be the base component of a larger building system.

using the silicon reference cell which had been calibrated and verified by the Fraunhofer Institute for Solar Energy Studies. The linear relationship between J_{SC} and light intensity which can be altered by a device and software called HelioCon (Voss electronic GmbH) was also used to set the solar simulator to 0.4, 0.6 and 0.8 suns, so that the devices could also be characterized under lower irradiances. Furthermore, for a non-tracking BICPV technology it is important to consider the case when the radiation is incident at non-normal angles. To investigate this quantitatively, the devices were placed on an inclined plane under the solar simulator which could have its angle with the horizontal varied (to give an effective angle of incidence the light equal to the angle of inclination from the horizontal). The modules were then characterised under 1 sun illumination following the same procedure as before at angles from 10° to 80° in intervals of 10°. On the other hand, for the EQE measurements, the Bentham PVE300 photovoltaic characterization system provides a tunable light source (within the range 300–2500 nm) based on a xenon-quartz tungsten halogen dual source and single monochromator (Bentham TMc 300). Through probes, a transformer pre-amplifier (Bentham S400 474) and signal detection unit (Bentham S400 417) it is able to measure the spectral response and EQE of PV cells. Another reference cell was used which included the spectral mismatch calculation in its calibration procedure. For this study, devices were placed on the stage and subject to 300–1100 nm illumination (in intervals of 10 nm) producing an EQE profile. Three measurements were taken for each device and a statistical analysis yielded average device performances.

3. Results

At 1 sun illumination the control CPV device was shown to have a PCE of 9.38%. From Fig. 4a) it can be seen as a higher PCE of 10.42% was observed for the best $NaYF_4$: Er^{3+}, Yb^{3+} device while for $Sr_4Al_{14}O_{25}$: Eu^{2+}, Dy^{3+} the highest efficiency measured was 9.92%, corresponding to the relative enhancements of 11.1% and 5.5%. The $NaYF_4$: Er^{3+}, Yb^{3+} device which achieved this best result was the doped optical coupling at 1% w/w whereas for $Sr_4Al_{14}O_{25}$: Eu^{2+}, Dy^{3+} it was the top doped concentrator. For both materials at most other doping levels and arrangements, efficiency was also improved by varying degrees of effectiveness, with the notable exceptions of 1% or 2% w/w doped optical coupling and homogenously doped concentrator for $Sr_4Al_{14}O_{25}$: Eu^{2+}, Dy^{3+} and bottom doped concentrator for $NaYF_4$: Er^{3+}, Yb^{3+} which all saw decreases in relative efficiency ranging from 0 to 2.3%.

J_{SC} improvements usually accompanied efficiency gains as can be observed by the current-voltage (I-V) curve intercepts. At 1 sun the $NaYF_4$: Er^{3+}, Yb^{3+} doped device which had the highest efficiency also had the highest J_{SC} of 77.78 mA/cm^2 (an 8.08% relative increase) and V_{OC} at 596.5 mV (a 1.9% relative increase). Although for the $Sr_4Al_{14}O_{25}$: Eu^{2+}, Dy^{3+} doped devices the greatest J_{SC} was observed for the device with the 2nd highest efficiency (bottom doped concentrator). Full tables for the efficiencies, J_{SC} and relative improvements of each device can be found in the supplementary information.

Upon illumination from lower intensity radiation, an interesting observation was made; both the relative efficiency and J_{SC} enhancements became more pronounced. This is demonstrated in Fig. 4b) which show the $NaYF_4$: Er^{3+}, Yb^{3+} doped device that had an 11.1% relative increase in efficiency at 1 sun, produced relative increases of 15.5% at 0.8 and 0.6 suns and 17.7% at 0.4 suns. A similar phenomenon was recorded for the best performing $Sr_4Al_{14}O_{25}$: Eu^{2+}, Dy^{3+} doped devices (Supplementary Fig. 12) although for the modules with doped optical couplings maximum relatively efficiency gains occurred at 0.8 suns. These variations could be down to the quantum efficiency of the DS or DC processes (and hence optical efficiency of the concentrator) being independent of light intensity whereas the PV cell's EQE and J_{SC} fall linearly with light intensity. This means the rare earth ions are able to keep producing high numbers of optimal wavelength photons at lower irradiances which leads to greater relative performance gains. However, for UC processes the quantum efficiency is expected to increase with light concentration [35], so may explain the localized peaks at 0.8 suns for the doped concentrator $NaYF_4$: Er^{3+}, Yb^{3+} devices where competing luminescent processes occur.

PCE and J_{SC} measurements were then obtained for the devices without concentrators. It was found at 1 Sun, the greatest efficiency for $Sr_4Al_{14}O_{25}$: Eu^{2+}, Dy^{3+} doped Sylgard was 16.31% at a doping concentration of 0.5% (a 2.1% relative improvement to un-doped Sylgard) whereas for $NaYF_4$: Er^{3+}, Yb^{3+} doped Sylgard was 16.75% at a doping concentration of 1.0% (a 4.8% relative improvement to un-doped Sylgard). These relative efficiency gains at varying irradiances could then be compared with the enhancements for the CPV cells with doped optical couplings (the same system but with an added concentrator).

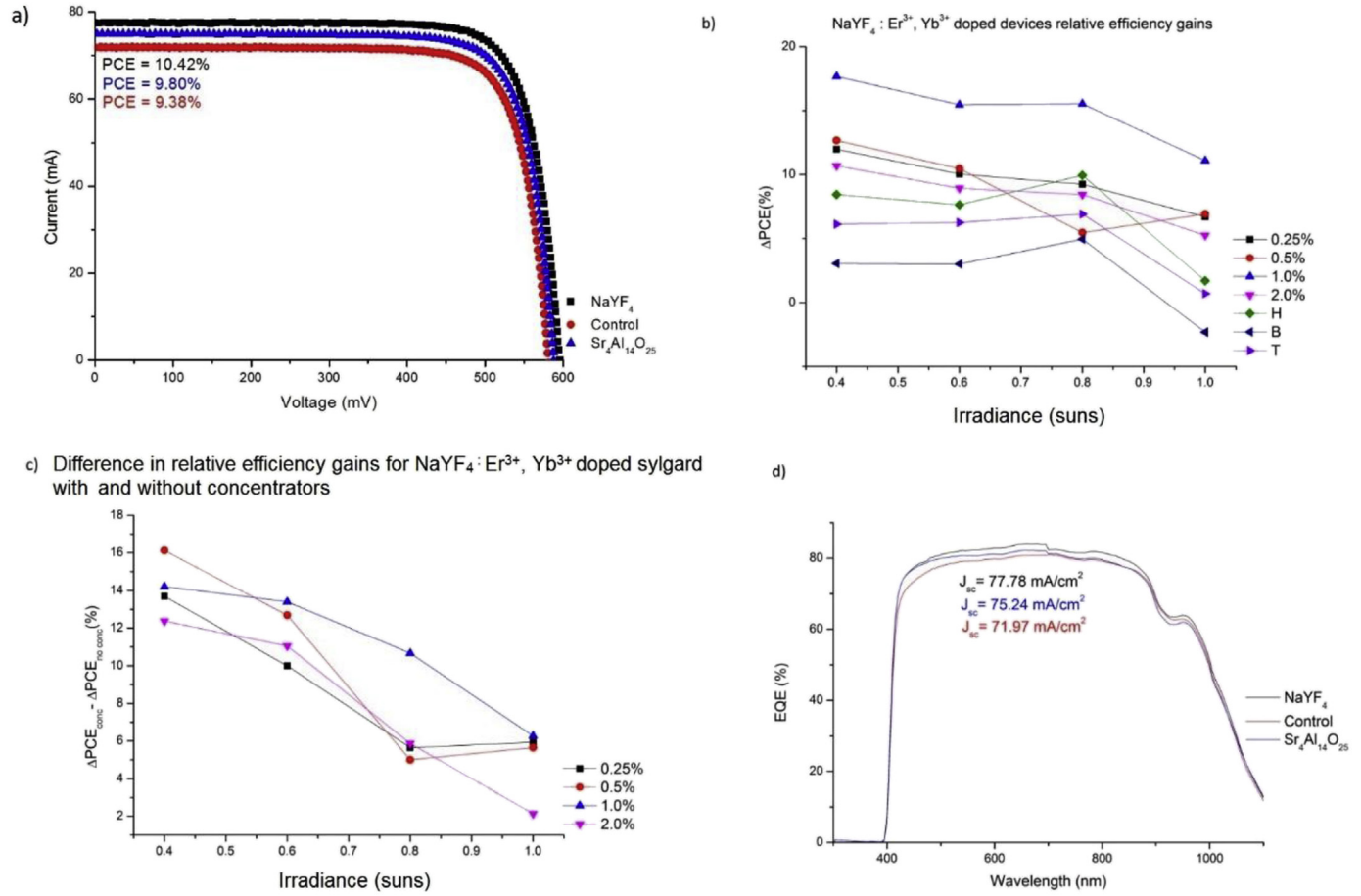

Fig. 4. Graphs to demonstrate the key findings. a) The I-V curves of the control device and $Sr_4Al_{14}O_{25}$: Eu^{2+}, Dy^{3+} and $NaYF_4$: Er^{3+}, Yb^{3+} devices with the highest power conversion efficiency. b) The relative efficiency gains for the $NaYF_4$: Er^{3+}, Yb^{3+} doped devices at irradiances (0.4, 0.6, 0.8 and 1 suns). c) A key result; the difference in relative efficiency improvements as compared to un-doped Sylgard for modules with (CPV) and without (PV) a concentrator for $NaYF_4$: Er^{3+}, Yb^{3+} doping. It can be observed that there is a greater relative enhancement in efficiency when concentrators are deployed, particularly at lower irradiances. d) EQE spectra for the $Sr_4Al_{14}O_{25}$: Eu^{2+}, Dy^{3+} and $NaYF_4$: Er^{3+}, Yb^{3+} CPV devices with the highest J_{SC}.

The difference in relative efficiency for these modules with and without the concentrator is outlined in Fig. 4c). This clearly shows the relative efficiency enhancements to be bigger for both materials (in almost all cases) when concentrators were placed on top of the solar cells. Yet again these differences were more pronounced at lower irradiances. For example, at 0.4 suns for 0.5% $NaYF_4$: Er^{3+}, Yb^{3+} doped Sylgard, with concentrator a relative increase in efficiency of 12.67% was observed and without concentrator a decrease of 3.46% was recorded, meaning the addition of an optic yielded a 16.13% greater relative enhancement in efficiency. This result means spectral conversion is a more promising method for improving the efficiency of CPV than non-concentrating PV, and therefore could lead to applications in BICPV where there is a need to increase power output per unit area (e.g. by higher module efficiencies), especially in areas of low irradiances.

The PCEs and relative PCE improvements for the $NaYF_4$: Er^{3+}, Yb^{3+} doped devices under varied angle of incidence illumination are presented in Fig. 5. Full numerical value tables, J_{SC} improvements and data for $Sr_4Al_{14}O_{25}$: Eu^{2+}, Dy^{3+} are available in the supplementary information. It can be seen from the data that the increased electrical performance also occurs at higher angles of incidence. In general, the larger the angle of incidence, the greater the relative PCE and J_{SC} improvement with some configurations such as the top and bottom doped concentrators performing better than under normal irradiance. It can be seen from Figures, that from 0° to 20° for both compounds and most configurations, the relative efficiency gains rise to a peak of +23.95% for the 1% optical coupling doped $NaYF_4$: Er^{3+}, Yb^{3+} containing device. Between 30° and 60°, the relative enhancements, though still positive, undergo an almost sinusoidal behaviour with increasing angle. Then finally, at high angles of incidence for most devices, there is a local minimum at 70° and maximum at 80°. For example, in top concentrator doped $NaYF_4$: Er^{3+}, Yb^{3+} devices, the relative PCE enhancement jumps from +8.14% at 70° to +41.71% at 80°.

The EQE spectra are presented in Fig. 4d) from which it can be seen that higher EQEs were recorded for the cells with higher power conversion efficiencies as expected and, of crucial interest to this study, an increased EQE was particularly observed in the regions of 400–500 nm for the doped devices, indicating successful photon conversion processes (DC and LDS) to improve electrical response to that part of the solar spectrum. The best performing $Sr_4Al_{14}O_{25}$: Eu^{2+}, Dy^{3+} showed an (absolute) 3.53% improvement in EQE at 450 nm and a larger enhancement of 3.96% was observed at the same wavelength for $NaYF_4$: Er^{3+}, Yb^{3+}. In the mid-range of the spectra (600–800 nm) the difference in EQE between the doped and un-doped becomes less sharp which is expected as little to no spectral conversion processes would occur under these excitation wavelengths. In some cases, the higher doping levels decrease the EQE further because of their lower optical transparency. Conversely, at the longer wavelengths (900–1100 nm), an improved EQE of up to 3.11% at 1050 nm is recorded for $NaYF_4$: Er^{3+}, Yb^{3+} doped optical coupling, whereas for $Sr_4Al_{14}O_{25}$: Eu^{2+}, Dy^{3+} 3 out of the 4 devices with a doped optical coupling showed a decrease in EQE at this wavelength. This hints that an additional spectral conversion process (UC) could be playing a role in the $NaYF_4$:

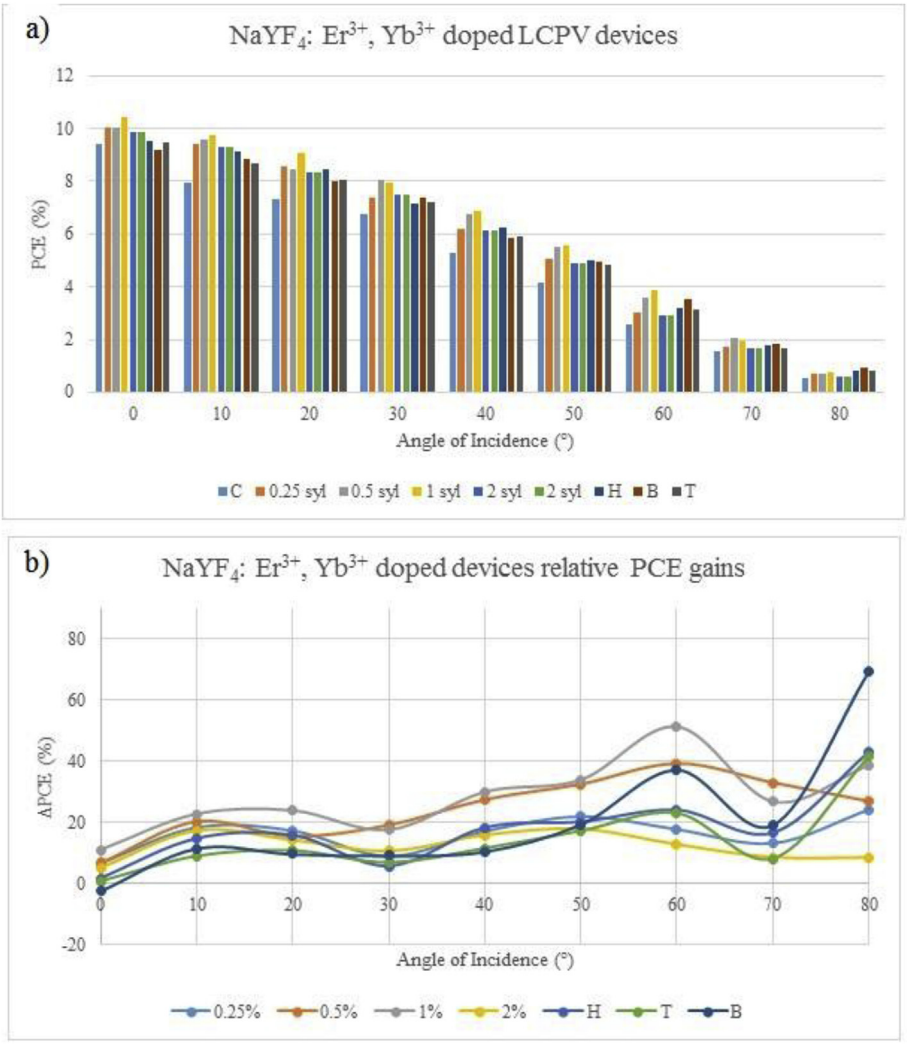

Fig. 5. Graphs to demonstrate the findings from the investigations of the effect of incidence angle on the $NaYF_4$: Er^{3+}, Yb^{3+} doped devices. a) The PCE of the $NaYF_4$: Er^{3+}, Yb^{3+} doped devices under 1 sun at angles of incidence from 0° to 80°. b) The relative PCE gains for the $NaYF_4$: Er^{3+}, Yb^{3+} doped devices under 1 sun at angles of incidence from 0° to 80°.

Er^{3+}, Yb^{3+} doped modules.

EQE spectra of devices without concentrators were also obtained as shown in Supplementary Figs. 18–19. These cells attained higher maximum EQEs and unlike the CPV modules, measured non-negligible EQEs in the 300–400 nm range. This is due to more radiation being available for the PV, since 300–400 nm wavelengths are almost completely absorbed by the 3-D optic (and hence unused by the cells beneath) and a fraction of photons of all energies are lost in the concentrator through unwanted absorption. Despite spectral conversion having a wider range of photons to increase EQE in non-concentrating PV, the relative EQE gains were smaller than in CPV. For example, without concentrators at wavelengths of 450 nm, the $Sr_4Al_{14}O_{25}$: Eu^{2+}, Dy^{3+} doped device's EQE was raised by up to 2.25% and 1.79% for $NaYF_4$: Er^{3+}, Yb^{3+}. These values are 36% and 55% lower than the EQE improvements achieved for each material with concentrators, supporting the hypothesis that spectral conversion was more effective at improving performance in CPV devices than in standard PV cells.

4. Discussion

It is important to understand the reasons behind these overall results in terms of the physical process stemming from material choice, doping concentrations and device geometry. $NaYF_4$: Er^{3+}, Yb^{3+} doped devices tended to outperform $Sr_4Al_{14}O_{25}$: Eu^{2+}, Dy^{3+} doped devices which could be due to their wider spectral absorption range, less scattering losses due to their smaller particle size and higher quantum efficiencies. However, the $Sr_4Al_{14}O_{25}$: Eu^{2+}, Dy^{3+} doped concentrators did achieve greater efficiency gains than $NaYF_4$: Er^{3+}, Yb^{3+} doped ones. This could be accounted for by self-absorption losses (that arise from the overlap between a rare earth ion's absorption and emission spectra) which will be more apparent in $NaYF_4$: Er^{3+}, Yb^{3+} than $Sr_4Al_{14}O_{25}$: Eu^{2+}, Dy^{3+}, especially over long optical path lengths, resulting in more photons lost whilst passing through the concentrator and hence the lower efficiency gains. A similar consideration could also explain why $NaYF_4$: Er^{3+}, Yb^{3+} performed best in the optical coupling; because of the layer's smaller size there was less path length for self-absorption losses to occur.

Also notably $Sr_4Al_{14}O_{25}$: Eu^{2+}, Dy^{3+} concentrators performed better when doped at the top or bottom of the concentrator. In previous studies, LSCs containing thin films doped with rare earth ions have been shown to yield greater performance improvements than homogenously doped concentrators, by ensuring absorption and emission events take place near the boundaries to minimize losses [36]. On the other hand, the $NaYF_4$: Er^{3+}, Yb^{3+} concentrators performed better when homogenously doped than when rare ions were confined to the top or base of the SEH, potentially because of their lower absorption coefficient across visible wavelengths which led to fewer optical losses over the whole spectrum (whilst still allowing more photons to be utilized for spectral

conversion processes).

The doping concentration of the rare earth ions is a major factor in the effectiveness of enhancing PV performance by spectral conversion, so is important to be optimized [37]. At high doping levels energy transfer between ions can lead to less efficient spectral conversion [38] and decrease the overall transparency of optical components, meaning less photons will reach the PV cell to generate photocurrent. Too low ratios evidently lead to insufficient spectral conversion, so a trade-off is needed to ensure a decent amount occurs but not to the detriment of PV cell performance at other wavelengths. For the doped optical couplings, $NaYF_4$: Er^{3+}, Yb^{3+} demonstrates this behavior well with a rise and fall in PV performance with increasing dopant concentration (since 0.5% and 2% w/w doping levels both had a lower device efficiency than the optimal 1% w/w), whereas for $Sr_4Al_{14}O_{25}$: Eu^{2+}, Dy^{3+} the lowest concentrations (0.25% and 0.5% w/w) yielded the best results, indicating competing processes such as scattering or that the ideal doping ratio could lie between or beneath these values. The optimal doping concentration may also be a factor of incident light intensity but for the materials and irradiances in this study, it appears to have little effect as the 1% w/w $NaYF_4$: Er^{3+}, Yb^{3+} and 0.25% and 0.5% w/w $Sr_4Al_{14}O_{25}$: Eu^{2+}, Dy^{3+} performed best at all illumination conditions.

As well as efficiency an important factor for BIPV modules is the cost per watt, typically \$4.1-\$24.5/W [39]. Given that an un-doped module cost \$51.81/W, by using a formula from [40] the best performing $Sr_4Al_{14}O_{25}$: Eu^{2+}, Dy^{3+} and $NaYF_4$: Er^{3+}, Yb^{3+} devices were calculated to have a cost per watt of \$49.15 and \$47.59 respectively (corresponding to reductions of 5.2% and 8.1%) and lowest cost per area of \$1350/m^2. These figures only take into account the material costs as used in the laboratory (not machinery, labour etc.) so could be significantly reduced for larger sized systems due to economies of scale. For reference, Wu et al. [41] calculated their tandem LSC devices could be produced on an industrial scale for \$5.01/m^2 compared to \$100/m^2 typical non-concentrating silicon PV. A prototype BICPV module to act as window façade based on this concentrator design[6] would contain 24 CPV cells in 0.031 m^2. Therefore, addition of $NaYF_4$: Er^{3+}, Yb^{3+} could lead to an increase in power per area from 25.7 W/m^2 to 28.4 W/m^2.

These preliminary results indicate that this technique of rare earth compound addition can also be used for enhancing the efficiency of BICPV modules when exposed to irradiance of off-normal angles of incidence. The greater enhancements could be due to the higher optical path lengths leading to increased absorption and re-emission of photons by the rare earth compounds within the concentrators. Although the relative gains reach maximum values, so like the doping ratio, there could be a trade off and hence optimum value for maximizing the useful spectral conversion and minimizing the parasitic visible absorption. In addition, the phenomenon of increased performance at the highest incidence angle (80°) for $NaYF_4$: Er^{3+}, Yb^{3+} could be due to a higher capture rate of glancing rays which are then redirected down towards the cell on emission.

If the promising potentials are to be realised suggestions must be made on where future studies involving these systems should focus. The primary aim should be optimization of the dopant materials for maximum spectral conversion and stability in regards to light-induced current on exposure. With a specific focus on $NaYF_4$: Er^{3+}, Yb^{3+} and $Sr_4Al_{14}O_{25}$: Eu^{2+}, Dy^{3+}, the particle size could be investigated as well as the doping level in the concentrators (two variables beyond the scope of this investigation). The use of photoluminescence spectroscopy could aid in determining the ideal configurations and decay profiles may be analyzed to determine the quantum efficiency and underlying mechanisms [42] (LDS or DC). Novel nanostructures [43,44] could be employed to increase emission (notwithstanding the need to minimize fabrication costs) and optical models [45,46] could accompany any studies in order to validate any experimental results. Furthermore, it would be of interest to see more molecules with spectral conversion properties (such as dyes and QDs) applied to 3-D concentrators of other designs in a comparative study between different configurations (with a focus on minimizing cost per watt and environmental impact), to determine the most suited material for wide-scale deployment of this technology. Finally, theoretical calculations, using accurate solar positioning/irradiance data, could be combined with a long-term experiment, observing the cumulative energy generated under real sunlight conditions over the course of a year which would give a deeper insight in to the realistic cost and performance benefits of this approach.

5. Conclusion

In conclusion, rare earth ion-containing compounds have been shown to improve performance in both PV and CPV single cell modules. Under 1 sun, $NaYF_4$: Er^{3+}, Yb^{3+} doped in the optical coupling was able to improve relative efficiency by 11.1% and doped into the top of the concentrator by 5.7%. At the same illumination conditions, relative efficiency improvements of up to 4.8% ($NaYF_4$: Er^{3+}, Yb^{3+}) and 2.1% ($Sr_4Al_{14}O_{25}$: Eu^{2+}, Dy^{3+}) were noted for the non-concentrating PV modules. Both the relative efficiency gains and the difference between these values for the CPV and PV module tended to be more amplified at lower irradiances (up to 16.1% for $NaYF_4$: Er^{3+}, Yb^{3+} at 0.4 suns) and performance improvements were observed under off-normal angle of incidence irradiation, demonstrating the effectiveness of this approach for CPV systems. EQE spectra were obtained to determine which range of wavelengths were contributing to these improved performances and results showed greater EQEs attained in the range 400–500 nm for both ions and to an extent at 900–1100 nm for $NaYF_4$: Er^{3+}, Yb^{3+}, indicating spectral conversion processes took place. Physical mechanisms responsible for the data were discussed and a basic cost analysis showed costs per watt could fall 8.1% for $NaYF_4$: Er^{3+}, Yb^{3+}. It is intended for this study to inspire the application of spectral conversion to more 3-D concentrators and through material optimization, to have a growing impact on the budding BICPV sector.

Acknowledgements

Funding for this study was provided by the Engineering and Physical Sciences Research Council (EP/J000345/2) and is gratefully acknowledged. The authors would also like to thank Mr James Yule, Dr Katie Shanks and Dr Shivangi Sharma from the University of Exeter for their general assistance towards ensuring quality device fabrication.

Appendix A. Supplementary data

Supplementary data to this article can be found online at https://doi.org/10.1016/j.solmat.2019.04.013.

References

[1] K. Shanks, S. Senthilarasu, T.K. Mallick, Optics for concentrating photovoltaics: trends, limits and opportunities for materials and design, Renew. Sustain. Energy Rev. 60 (2016) 394–407 https://doi.org/10.1016/j.rser.2016.01.089.
[2] W.T. Xie, Y.J. Dai, R.Z. Wang, K. Sumathy, Concentrated solar energy applications using Fresnel lenses: a review, Renew. Sustain. Energy Rev. 15 (2011) 2588–2606 https://doi.org/10.1016/j.rser.2011.03.031.
[3] A.M. Manokar, D. Prince Winston, M. Vimala, Performance analysis of parabolic trough concentrating photovoltaic thermal system, Proc. Tech. 24 (2015) 4850491 https://doi.org/10.1016/j.protcy.2016.05.083.
[4] A.H. Jaaz, H.A. Hasan, K. Sopian, M.H.B.H. Ruslan, S.H. Zaidi, Design and development of compound parabolic concentrating for photovoltaic solar collector: Review, Renew. Sustain. Energy Rev. 76 (2017) 1108–1121 https://doi.org/10.1016/j.rser.2017.03.127.
[5] K. Shanks, S. Senthilarasu, R.H. ffrench-Constant, T.K. Mallick, White butterflies as solar photovoltaic concentrators, Sci. Rep. 5 (2015) 12267 https://doi.org/10.1038/srep12267.
[6] N. Sellami, T.K. Mallick, D.A. McNeil, Optical characterisation of 3-D static solar concentrator, Energy Convers. Manag. 64 (2012) 579–586 https://doi.org/10.1016/j.enconman.2012.05.028.
[7] X. Huang, S. Han, W. Huang, X. Liu, Enhancing solar cell efficiency: the search for luminescent materials as spectral converters, Chem. Soc. Rev. 42 (2013) 173–201 https://doi.org/10.1039/C2CS35288E.
[8] H. Cotal, C. Fezter, J. Boisvert, G. Kinsey, R. King, P. Herbert, H. Yoon, N. Karam,

III-V multijunction solar cells for concentrating photovoltaics, Energy Environ. Sci. 2 (2009) 174–192 https://doi.org/10.1039/B809257E.
[9] T.K. Todorov, D.M. Bishop, Y.S. Lee, Materials perspectives for next-generation low-cost tandem solar cells, Sol. Energ. Mater. Sol. Cells 180 (2018) 350–357 https://doi.org/10.1016/j.solmat.2017.07.033.
[10] D.H. Weingarten, M.D. LaCount, J. van de Lagemaat, G. Rumbles, M.T. Lusk, S.E. Shaheen, Experimental demonstration of photon upconversion via cooperative energy pooling, Nat. Commun. 8 (2017) 14808 https://doi.org/10.1038/ncomms14808.
[11] D.C. Yu, R. Martín-Rodríguez, Q.Y. Zhang, A. Meijerink, F.T. Rabouw, Multi-photon quantum cutting in $Gd_2O_2S:Tm^{3+}$ to enhance the photo-response of solar cells, Light Sci. Appl. 4 (2015) e344 https://doi.org/10.1038/lsa.2015.117.
[12] E. Klampaftis, D. Ross, K.R. McIntosh, B.S. Richards, Enhancing the performance of solar cells via luminescent down-shifting of the incident spectrum: a review, Sol. Energ. Mater. Sol. Cells 93 (2009) 1182–1194 https://doi.org/10.1016/j.solmat.2009.02.020.
[13] M.A. Green, S.P. Bremner, Energy conversion approaches and materials for high-efficiency photovoltaics, Nat. Mater. 16 (2017) 23–24 https://doi.org/10.1038/nmat4676.
[14] W. Zou, C. Visser, J.A. Maduro, M.S. Pshenichnikov, J.C. Hummelen, Broadband dye sensitized upconversion of near-infrared light, Nat. Photon. 6 (2012) 560–564 https://doi.org/10.1038/nphoton.2012.158.
[15] D. Ross, D. Alonso-Álvarez, E. Klampaftis, J. Fritsche, M. Bauer, M.G. Debije, R.M. Fifield, B.S. Richards, The impact of luminescent down shifting on the performance of CdTe photovoltaics: impact of the module vintage, IEEE J. Photovolt. 4 (2014) 457–464 https://doi.org/10.1109/JPHOTOV.2013.2282896.
[16] T.S. Parel, L. Danos, T. Markvart, Application of concentrating luminescent down-shifting structures to CdS/CdTe solar cells with poor short wavelength response, Sol. Energ. Mater. Sol. Cells 140 (2015) 306–311 https://doi.org/10.1016/j.solmat.2015.04.026.
[17] Z. Deutsch, L. Neeman, D. Oron, Luminescence upconversion in colloidal double quantum dots, Nat. Nanotechnol. 8 (2013) 649–653 https://doi.org/10.1038/nnano.2013.146.
[18] A. Teitelboim, D. Oron, Broadband near-infrared to visible upconversion in quantum dot–quantum well heterostructures, ACS Nano 10 (2016) 446–452 https://doi.org/10.1021/acsnano.5b05329.
[19] S. Kalytchuk, S. Gupta, O. Zhovtiuk, A. Vaneski, S.V. Kershaw, H. Fu, Z. Fan, E.C.H. Kwok, C.F. Wang, W.Y. Teoh, A.L. Rogach, Semiconductor nanocrystals as luminescent down-shifting layers to enhance the efficiency of thin-film CdTe/CdS and crystalline Si solar cells, J. Phys. Chem. C 118 (2014) 16393–16400 https://doi.org/10.1021/jp410279z.
[20] L.D. Sun, H. Dong, P.Z. Zhang, C.H. Yan, Upconversion of rare Earth nanomaterials, Annu. Rev. Phys. Chem. 66 (2015) 619–642 https://doi.org/10.1146/annurev-physchem-040214-121344.
[21] Y. Zhong, Z. Ma, S. Zhu, J. Yue, A.L. Antaris, J. Yuan, R. Cui, H. Wan, Y. Zhou, W. Wang, N.F. Huang, J. Luo, Z. Hu, H. Dai, Boosting the down-shifting luminescence of rare-earth nanocrystals for biological imaging beyond 1500 nm, Nat. Commun. 8 (2017) 737 https://doi.org/10.1038/s41467-017-00917-6.
[22] X. Hou, T. Xuan, H. Sun, X. Chen, H. Li, L. Pan, High-performance perovskite solar cells by incorporating a $ZnGa_2O_4:Eu^{3+}$ nanophosphor in the mesoporous TiO_2 layer, Sol. Energ. Mater. Sol. Cells 149 (2016) 121–127 https://doi.org/10.1016/j.solmat.2016.01.021.
[23] R. Lopez-Delgado, Y. Zhou, A. Zazueta-Raynaud, H. Zhao, J.E. Pelayo, A. Vomiero, M.E. Álvarez-Ramos, F. Rosei, A. Ayon, Enhanced conversion efficiency in Si solar cells employing photoluminescent down-shifting CdSe/CdS core/shell quantum dots, Sci. Rep. 7 (2017) 14104 https://doi.org/10.1038/s41598-017-14269-0.
[24] G.E. Arnaoutakis, J. Marques-Hueso, A. Ivaturi, S. Fischer, J.S. Goldschmidt, K.W. Krämer, B.S. Richards, Enhanced energy conversion of up-conversion solar cells by the integration of compound parabolic concentrating optics, Sol. Energy Mater. Sol. Cells 140 (2015) 217–223 https://doi.org/10.1016/j.solmat.2015.04.020.
[25] S. Asahi, H. Teranishi, K. Kusaki, K. Kaisu, T. Kita, Two-step photon up-conversion solar cells, Nat. Commun. 8 (2016) 14962 https://doi.org/10.1038/ncomms14962.
[26] W.H. Weber, J. Lambe, Luminescent greenhouse collector for solar radiation, Appl. Optic. 15 (1976) 2299–2300 https://doi.org/10.1364/AO.15.002299.
[27] F. Meinardi, F. Bruni, S. Brovelli, Luminescent solar concentrators for building-integrated photovoltaics, Nat. Rev. Mat. 2 (2017) 17072 https://doi.org/10.1038/natrevmats.2017.72.
[28] F. Meinardi, H. McDaneil, F. Carulli, A. Colombo, K.A. Velizhanin, N.S. Makarov, R. Simonutti, V.I. Klimov, S. Brovelli, Highly efficient large-area colourless luminescent solar concentrators using heavy-metal-free colloidal quantum dots, Nat. Nanotechnol. 10 (2015) 878-876 https://doi.org/10.1038/nnano.2015.178.
[29] F. Meinardi, S. Eherenberg, L. Dhamo, F. Carulli, F. Bruni, R. Simonutti, U. Kortshagen, S. Brovelli, Highly efficient luminescent solar concentrators based on earth-abundant indirect-bandgap silicon quantum dots, Nat. Photon. 11 (2017) 177–186 https://doi.org/10.1038/nphoton.2017.5.
[30] C. Li, W. Chen, D. Wu, D. Quan, Z. Zhou, J. Hao, J. Qin, Y. Lie, Z. He, K. Wang, Large Stokes shift and high efficiency luminescent solar concentrator incorporated with $CuInS_2/ZnS$ quantum dots, Sci. Rep. 5 (2015) 17777 https://doi.org/10.1038/srep17777.
[31] H. Li, K. Wu, J. Lim, H.J. Song, V.I. Klimov, Doctor-blade deposition of quantum dots onto standard window glass for low-loss large-area luminescent solar concentrators, Nat. Energ. 1 (2016) 16157 https://doi.org/10.1038/nenergy.2016.157.
[32] B. Qu, Y. Jiao, S. He, Y. Zhu, P. Liu, J. Sun, J. Lu, X. Zhang, Improved performance of a-Si: H solar cell by using up-conversion phosphors, J. Alloy. Comp. 658 (2016) 848–853 https://doi.org/10.1016/j.jallcom.2015.11.024.
[33] L. Aarts, B.M. van der Ende, A. Meijerink, Downconversion for solar cells in $NaYF_4$: Er,Yb, J. Appl. Phys.. 106 (2016) 023522https://doi.org/10.1063/1.3177257.
[34] H. Sun, L. Pan, G. Zhu, X. Piao, L. Zhang, Z. Sun, Long afterglow $Sr_4Al_{14}O_{25}$:Eu,Dy phosphors as both scattering and down converting layer for CdS quantum dot-sensitized solar cells, Dalton Trans. 43 (2014) 14936 https://doi.org/10.1039/c4dt01276c.
[35] B.S. Richards, Enhancing the performance of silicon solar cells via the application of passive luminescence conversion layers, Sol. Energ. Mater. Sol. Cells 90 (2006) 2329–2337 https://doi.org/10.1016/j.solmat.2006.03.035.
[36] M.H. Hughes, D.A. Borca-Tasciuc, D. Kaminski, Highly efficient luminescent solar concentrators employing commercially available luminescent phosphors, Sol. Energ. Mater. Sol. Cells 171 (2017) 293–301 https://doi.org/10.1016/j.solmat.2017.06.018.
[37] S. Chandra, S.J. McCormack, M. Kennedy, J. Doran, Quantum dot solar concentrator: optical transportation and doping concentration optimization, Sol. Energy 115 (2015) 552–561 https://doi.org/10.1016/j.solener.2015.01.048.
[38] F. Vetrone, R. Naccache, V. Mahalingam, C.G. Morgan, J.A. Capobianco, The active-core/active-shell approach: a strategy to enhance the upconversion luminescence in lanthanide-doped nanoparticles, Adv. Funct. Mater. 19 (2009) 2924–2929 https://doi.org/10.1002/adfm.200900234.
[39] R.J. Yang, P.X.W. Zou, Building integrated photovoltaics (BIPV): costs, benefits, risks, barriers and improvement strategy, Int. J. Constr. Manag. 16 (2016) 39–53 https://doi.org/10.1080/15623599.2015.1117709.
[40] J. Day, S. Senthilarasu, T.K. Mallick, Improving spectral modification for applications in solar cells: a review, Renew. Energy 132 (2019) 186–205 https://doi.org/10.1016/j.renene.2018.07.101.
[41] K. Wu, H. Li, V.I. Kilmov, Tandem luminescent solar concentrators based on engineered quantum dots, Nat. Photon. 12 (2018) 105–110 https://doi.org/10.1038/s41566-017-0070-7.
[42] Y. Li, X. Wei, H. Chen, Y. Pan, Y. Ji, Near-infrared downconversion through host sensitized energy transfer in Yb^{3+}-doped $Na_2YMg_2(VO_4)_3$, Phys. B 478 (2015) 95–98 https://doi.org/10.1016/j.physb.2015.09.011.
[43] W.L. Barnes, A. Dereux, T.W. Ebbesen, Surface plasmon subwavelength optics, Nat 424 (2003) 824–830 https://doi.org/10.1038/nature01937.
[44] S.M. El-Bashir, F.M. Barakat, M.S. AlSalhi, Double layered plasmonic thin-film luminescent solar concentrators based on polycarbonate supports, Renew. Energy 63 (2014) 642–649 https://doi.org/10.1016/j.renene.2013.10.014.
[45] R. Rothemund, Optical modelling of the external quantum efficiency of solar cells with luminescent down-shifting layers, Sol. Energ. Mater. Sol. Cells 120 (2014) 616–621 https://doi.org/10.1016/j.solmat.2013.10.004.
[46] H. Ahmed, S.J. McCormack, J. Doren, External quantum efficiency improvement with luminescent downshifting layers: experimental and modelling, Int. J. Spectrosc. (2016) 8543475 2016 https://doi.org/10.1155/2016/8543475.